This is an open access article published under an ACS AuthorChoice License, which permits copying and redistribution of the article or any adaptations for non-commercial purposes.

ACS AUTHORCHOICE

ACS OMEGA

http://pubs.acs.org/journal/acsodf

Article

Identifying Specific Combinations of Matrix Properties that Promote Controlled and Sustained Release of a Hydrophobic Drug from Electrospun Meshes

Nikhita Joy and Satyavrata Samavedi*

Cite This: *ACS Omega* 2020, 5, 15865−15876

Read Online

ACCESS | Metrics & More | Article Recommendations | Supporting Information

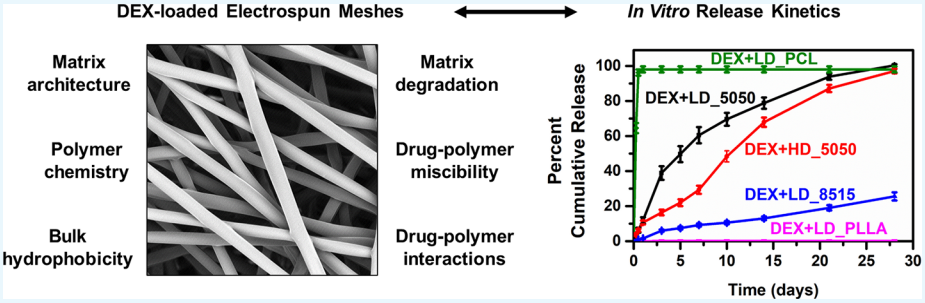

ABSTRACT: Despite advances in the development of degradable polymers for drug delivery, effective translation of drug-loaded materials is often hindered due to a poor understanding of matrix property combinations that promote controlled and sustained release. In this study, we investigated the influence of dominant factors on the release of a hydrophobic glucocorticoid dexamethasone (DEX) from electrospun meshes. Polycaprolactone meshes released 98% of the drug within 24 h, while poly(L-lactide) meshes exhibited negligible release even after 28 days despite both polymers being slow-degrading. Differences in drug-polymer interactions and drug-polymer miscibility—but neither matrix degradation nor differences in bulk hydrophobicity—influenced DEX release from these semi-crystalline matrices. Poly(D,L-lactide-*co*-glycolide) 50:50 meshes possessing two different fiber diameters exhibited a sequential burst and sustained release, while poly(D,L-lactide-*co*-glycolide) 85:15 meshes cumulatively released 26% drug in a controlled manner. Although initial drug release from these matrices was driven by differences in matrix architecture and solid-state drug solubility, release toward the later stages was influenced by a combination of fiber swelling and matrix degradation as evidenced by gross and microstructural changes to the mesh network. We suggest that drug release from polymeric matrices can be better understood via investigation of critical matrix characteristics influencing release, as well as concomitant examination of drug-polymer interactions and miscibility. Our findings offer rational matrix design criteria to achieve controlled/extended drug release for promoting sustained biological responses.

Downloaded via INDIAN INST OF TECH HYDERABAD on November 9, 2022 at 04:15:52 (UTC).
See https://pubs.acs.org/sharingguidelines for options on how to legitimately share published articles.

1. INTRODUCTION

Chronic inflammation is a critical factor implicated in several diseases and accounts for 3 in 5 deaths worldwide.[1] Unlike an acute inflammatory response that typically resolves within several days, chronic tissue inflammation can extend over months or even years, progressively worsening with time and causing extensive and in some cases irreversible, tissue-level damage.[1,2] To combat long-term inflammation in conditions such as arthritis, glucocorticoids are often administered systemically (e.g., oral, intravenous) typically at high doses, which can lead to high absorption into circulation, poor local availability and also promote adverse side effects such as osteoporosis, cushingoid state, and adrenal suppression.[3] In contrast, incorporating the drug within degradable polymeric matrices can offer controlled and localized release while overcoming the limitations associated with systemic delivery and permitting a reduction in drug loading.[4,5] The timescale of drug release from engineered matrices depends upon the mode of testing and the desired biological outcomes. For example, drugs can be released over the course of a few days to assess macrophage polarization in vitro[6] and up to a few months to assess suppression of chronic inflammation in vivo.[7,8] Since the release kinetics of drugs from biomaterial matrices is affected by a combination of several complex factors, including matrix properties, drug loading, and drug-matrix interactions,[9] a deeper understanding of specific combinations of matrix properties that promote controlled and sustained release can

Received: March 3, 2020
Accepted: June 9, 2020
Published: June 22, 2020

© 2020 American Chemical Society

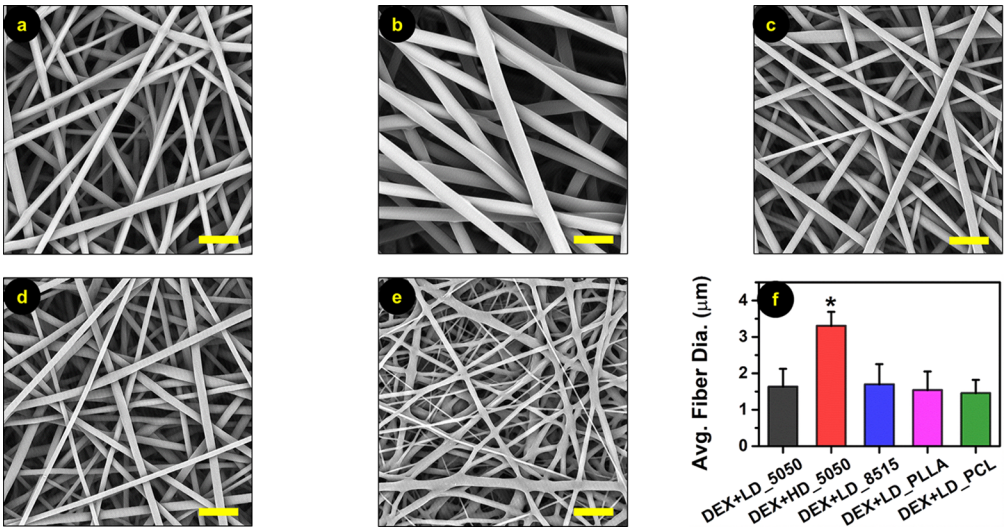

Figure 1. (a–e) SEM micrographs of DEX-incorporated meshes: (a) DEX+LD_5050, (b) DEX+HD_5050, (c) DEX+LD_8515, (d) DEX +LD_PLLA, and (e) DEX+LD_PCL. Scale bars correspond to 10 μm. (f) Average fiber diameter for the experimental groups. An asterisk symbol indicates statistical significance compared to all other samples ($p < 0.01$).

enable the rational design of materials for combating chronic inflammation. Judicious choice of material properties is particularly critical to avoid undesirable release kinetics (e.g., large burst release) and low long-term bioavailability. In this study, we systematically investigate the combined roles of polymer chemistry, matrix architecture, bulk matrix hydrophobicity, fiber swelling, matrix degradability, and drug-polymer interactions on the in vitro release kinetics of an anti-inflammatory drug dexamethasone (DEX) over 4 weeks. We identify critical factors that promote extended and controlled drug release to potentially result in sustained biological responses.

Poly α-esters are preferred for the preparation of drug carrier matrices due to their ability to degrade into non-toxic end products.[10] Further, the ability to alter their degradation rates by varying the molecular weight, crystallinity, and backbone chemistry allows poly α-esters to be effectively used in a variety of applications that require sustained release.[11] Among several approaches for processing synthetic polymers into drug-loaded implantable matrices/patches, electrospinning is a simple and versatile technique that enables the fabrication of non-woven fibrous matrices with high drug loading/encapsulation.[12] The properties of electrospun meshes can be systematically modulated both in situ and post-fabrication.[13] By modulating matrix properties as well as altering the modes of drug loading, electrospun meshes can be used to achieve differential drug release kinetics.[14,15]

Previous studies have reported the preparation and evaluation of DEX-loaded microparticles,[16] electrospun fibers,[17] micelles,[18] in situ forming implants,[19] and injectable colloidal gels[20] for specific biomedical applications such as bone tissue engineering and treating inflammatory ocular diseases. However, only a few studies have investigated the influence of a limited number of electrospun matrix properties on drug release. For example, Vacanti et al. showed differential release kinetics of DEX from two electrospun matrices possessing different chemistries,[8] while Kharaziha et al. reported the influence of fiber orientation on DEX release.[21] In another study, Li et al. demonstrated that the incorporation of a water-soluble polymer into electrospun matrices provided additional control over the release kinetics of DEX.[22] Despite these reports, how combinations of physicochemical, thermal, and architectural matrix properties together orchestrate DEX release from electrospun meshes, as well as the relative temporal dominance of specific factors, have not been investigated. Moreover, mechanistic insights to enable a judicious combination of electrospun matrix properties for promoting controlled and sustained release of DEX have not been reported.

The central hypothesis of this study is that a deeper understanding of combinations of electrospun matrix properties and associated factors that influence the release of hydrophobic drugs can aid the rational design of polymeric matrices for applications requiring extended release. Accordingly, DEX was independently incorporated into four poly α-esters, viz., poly(D,L-lactide-*co*-glycolide) 50:50, poly(D,L-lactide-*co*-glycolide) 85:15, poly(L-lactide), and polycaprolactone with similar molecular weights, and the drug-loaded polymeric solutions were processed to result in electrospun meshes possessing varying properties. DEX-loaded and no-drug control samples were characterized to establish differences in mesh architecture, bulk hydrophobicity, gross/microstructural changes in aqueous environments (as a qualitative assessment of matrix degradability), thermal properties, possible drug-polymer interactions, and drug-polymer miscibility. Subsequently, in vitro release of DEX from the electrospun matrices was investigated over 28 days. To the best of our knowledge, ours is the first comprehensive report providing systematic insights into the relative dominance of specific matrix properties and associated factors driving the release of a hydrophobic glucocorticoid from synthetic electrospun meshes fabricated using poly α-esters. The findings from this study can aid the effective use of drug-loaded bioactive materials in biomedical applications, including the development of materials to combat chronic inflammation through localized, controlled, and sustained release of DEX. Localized DEX release from meshes can also minimize inflammation arising from invasive surgical implantation (e.g., subcutaneous, intramuscular), while sustained release can

https://dx.doi.org/10.1021/acsomega.0c00954
ACS Omega 2020, 5, 15865−15876

mitigate the risk of chronic inflammation that can potentially arise from the use of degradable synthetic materials.[8,23]

2. RESULTS

2.1. Analysis of Mesh Architecture. Polymer solutions containing 8.5 mg/mL DEX were electrospun to result in five different fibrous meshes possessing bead-free smooth fibers (Figure 1a−e). The diameter distribution for all DEX-loaded samples is presented in Figure S1, Supporting Information. Specifically, samples designated DEX+LD_5050 (Figure 1a), DEX+LD_8515 (Figure 1c), DEX+LD_PLLA (Figure 1d), and DEX+LD_PCL (Figure 1e) possessed similar diameters, viz., 1.63 ± 0.49, 1.70 ± 0.55, 1.54 ± 0.51, and 1.45 ± 0.37 μm, respectively (Figure 1f). A higher polymer concentration used for preparing the DEX+HD_5050 samples (Figure 1b) resulted in a significantly higher diameter of 3.30 ± 0.39 μm compared to the rest of the groups ($p < 0.01$). Further, SEM micrographs at higher magnification revealed drug aggregates on the surface of a DEX+LD_PCL sample, which were not observed in the LD_PCL control group (Figure S2, Supporting Information).

DEX-loaded meshes were obtained by electrospinning for 60 min, and the mesh thicknesses were found to be 190 ± 23, 235 ± 62, 160 ± 4, 171 ± 16, and 251 ± 24 μm for the DEX+LD_5050, DEX+HD_5050, DEX+LD_8515, DEX+LD_PLLA, and DEX+LD_PCL, respectively (Figure S3, Supporting Information). Although the thicknesses of the DEX+HD_5050 and DEX+LD_PCL samples were slightly higher than the rest of the groups, these differences were not statistically significant. Subsequent porosity measurements using a standard gravimetric method revealed values of 0.83 ± 0.01, 0.81 ± 0.06, 0.80 ± 0.003, 0.81 ± 0.02, and 0.89 ± 0.01 for the DEX+LD_5050, DEX+HD_5050, DEX+LD_8515, DEX+LD_PLLA, and DEX+LD_PCL, respectively (Figure 2), with no significant differences across the groups.

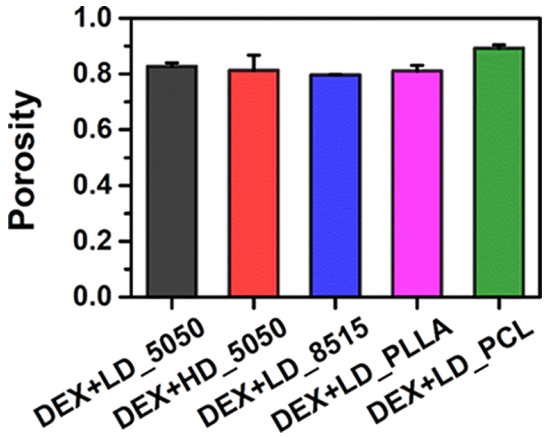

Figure 2. Porosity of DEX-loaded electrospun meshes.

2.2. Characterization of Relative Bulk Hydrophobicity. Differences in mesh wettability and consequent solvent diffusion were evaluated by measuring the relative bulk hydrophobicity of electrospun meshes using a technique that relies upon differential swelling in solvents of variable polarities, viz., 2-propanol and water. Swelling ratios thus obtained were used to calculate a hydrophobicity index (H-index) for each experimental group. The H-index of LD_PCL was 3.56 ± 0.91 and significantly higher than the other samples ($p < 0.01$) (Figure 3), while the H-indices of the rest of the samples—1.30 ± 0.02 for LD_5050, 1.84 ± 0.08 for HD_5050, 1.36 ± 0.10 for LD_8515, and 1.58 ± 0.02 for LD_PLLA—were not significantly different from each other.

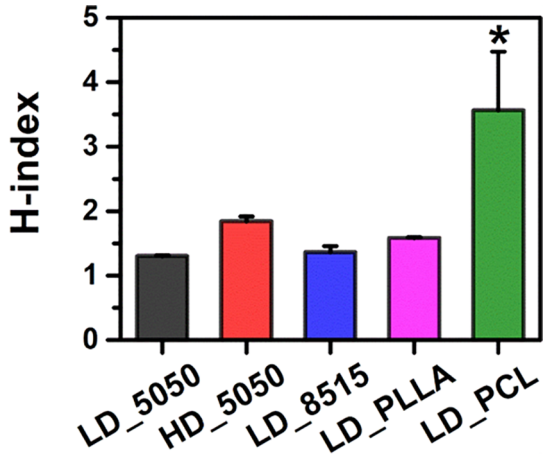

Figure 3. Relative hydrophobicity indices (H-index) of electrospun samples. An asterisk symbol indicates statistical significance compared to the rest of the samples ($p < 0.01$).

2.3. Qualitative Assessment of Mesh Degradation via Evaluation of Structural Changes to Fiber Network and Mesh Morphology. Gross morphological changes in the electrospun meshes post-soaking in PBS at 37 °C for 28 days were evaluated by periodic inspection of samples, while changes to the microstructure of the fibrous networks were assessed via SEM. After one day in PBS, the LD_5050 and HD_5050 samples underwent gross macroscopic shrinkage due to the onset of pore closure (Figure 4). By day 7, further pore closure and concomitant fiber swelling were observed in both samples (Figure 5). By day 28, the LD_5050 and HD_5050 meshes had shrunk further and disintegrated, with both samples exhibiting fused rugged fibers under SEM. While the LD_8515 samples had also shrunk significantly by day 7 (Figure 4), they exhibited pore closure to a lesser extent compared to the LD_5050 and HD_5050 samples (Figure 5). However, complete pore closure was noted in the LD_8515

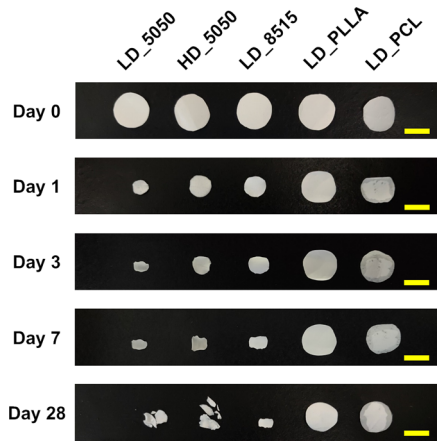

Figure 4. Macroscopic images of electrospun meshes immersed in PBS at 37 °C for 1, 3, 7, and 28 days. Scale bars correspond to 1 cm.

https://dx.doi.org/10.1021/acsomega.0c00954
ACS Omega 2020, 5, 15865−15876

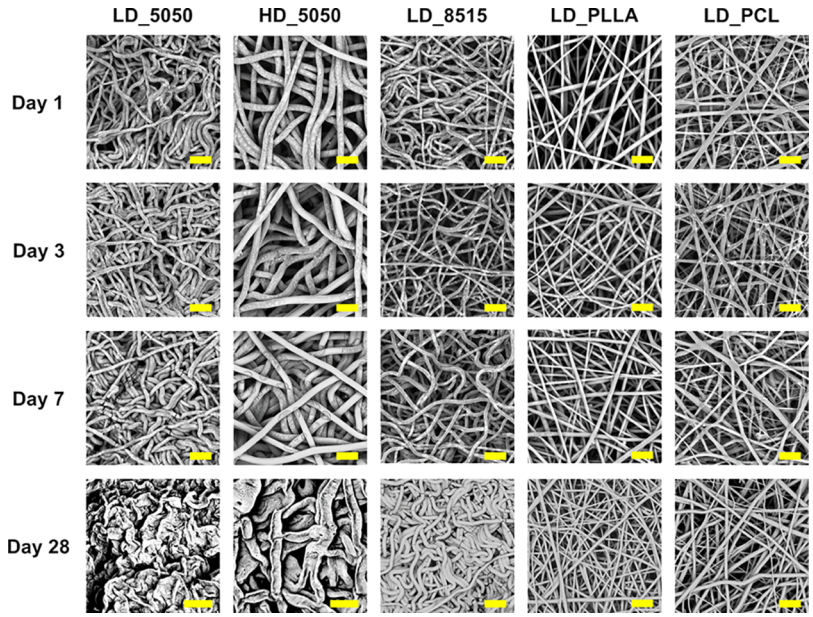

Figure 5. SEM micrographs of electrospun samples immersed in PBS at 37 °C for 1, 3, 7, and 28 days. Scale bars correspond to 10 μm. The particles on the fibers are salt deposits from PBS post-drying.

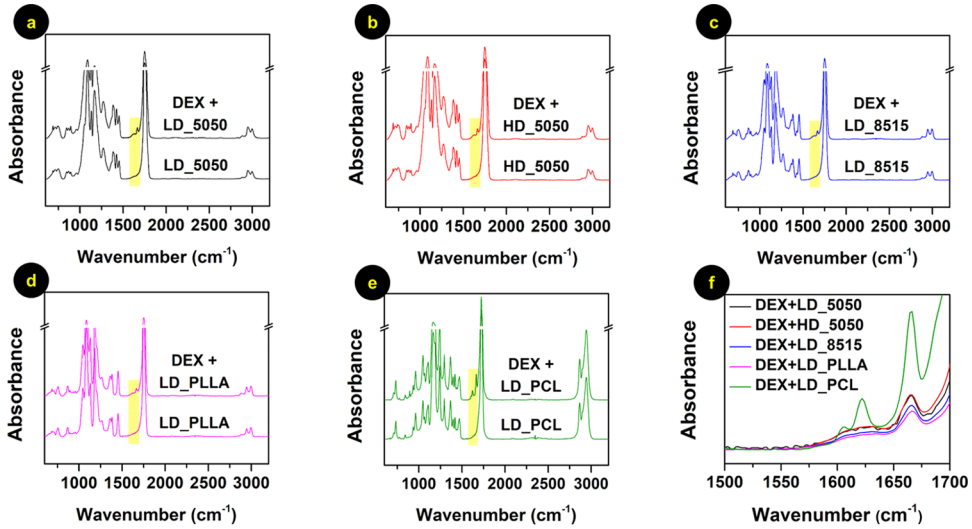

Figure 6. (a−e) ATR-FTIR spectroscopic data of meshes with and without DEX: (a) DEX+LD_5050 and LD_5050, (b) DEX+HD_5050 and HD_5050, (c) DEX+LD_8515 and LD_8515, (d) DEX+LD_PLLA and LD_PLLA, and (e) DEX+LD_PCL and LD_PCL. (f) Magnified spectroscopic data between 1500 and 1700 cm^{-1} for electrospun meshes incorporated with DEX.

samples by day 28. In contrast, gross macroscopic changes (Figure 4), fiber swelling, and evidence of microstructural changes to the fibrous network were not observed in both the LD_PLLA and LD_PCL samples throughout the study period (Figure 5).

2.4. Drug Presence Determined by ATR-FTIR Spectroscopy. ATR-FTIR was used to confirm fiber chemistry and the presence of DEX in the fibrous meshes (Figure 6). The characteristic absorption peak associated with deformational vibration of the C−H bond on the O−CH_2− group for poly α-esters was observed between 1365 and 1452 cm^{-1} in all control and DEX-loaded samples, and the peak corresponding to ester carbonyl (C═O) was also noted between 1722 and 1751 cm^{-1}. Only in the drug-loaded samples, the most intense characteristic peak of DEX corresponding to an unsaturated carbonyl group was observed at 1666.39 cm^{-1} (Figure 6a−e). Moreover, other DEX peaks at 1606.60 and 1622.03 cm^{-1} for C═C bonds were prominent only in DEX+LD_PCL samples (Figure 6f). However, no significant peak shifts were observed in any of the DEX-loaded samples compared to the controls.

2.5. Analysis of Thermal Behavior and Determination of Important Thermal Properties. TGA was performed on the electrospun samples without DEX to determine the moisture content and the onset of decomposition. The analysis revealed less than 3.5% (w/w) unbound water in all samples, and decomposition onset temperatures of 246.8, 250.4, 257.6, 254.3, and 342.5 °C for the LD_5050, HD_5050, LD_8515, LD_PLLA, and LD_PCL samples, respectively (Figure S4, Supporting Information). Based on 5% weight loss, the upper limit of the temperature range was chosen for further analysis with DSC.

https://dx.doi.org/10.1021/acsomega.0c00954
ACS Omega 2020, 5, 15865−15876

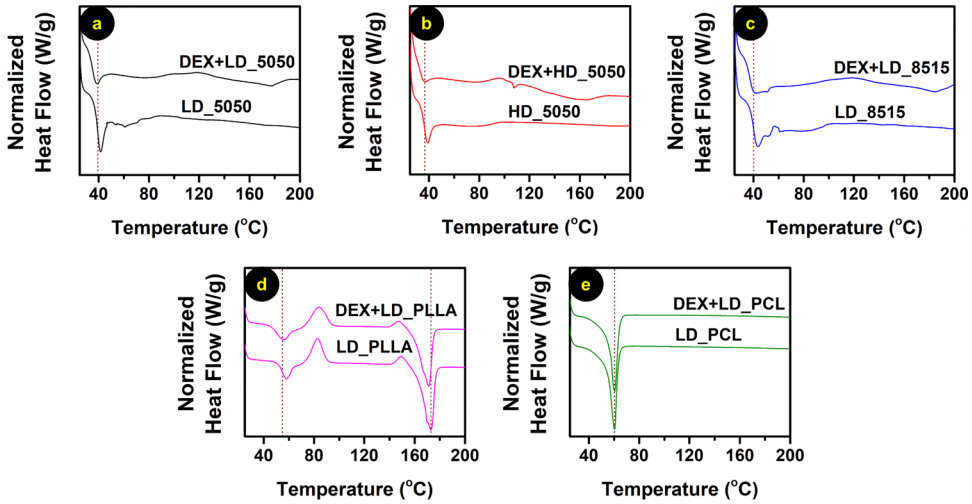

Figure 7. DSC thermograms of meshes with and without DEX (Exo ↑): (a) DEX+LD_5050 and LD_5050, (b) DEX+HD_5050 and HD_5050, (c) DEX+LD_8515 and LD_8515, (d) DEX+LD_PLLA and LD_PLLA, and (e) DEX+LD_PCL and LD_PCL.

For the amorphous polymers tested, DSC analysis helped identify the T_g values of LD_5050, HD_5050, and LD_8515 samples at 39.5, 36.7, and 40.3 °C, respectively (Figure 7a−c). For the LD_8515 sample, an additional cold crystallization peak at 55.9 °C associated with a ΔH_{cc} of 0.77 J g^{-1} was also observed. Compared to the no-drug controls, T_g values for the DEX-loaded samples reduced by 4.1 °C for DEX+LD_5050, 4.0 °C for DEX+HD_5050, and 3.1 °C for DEX+LD_8515. Likewise, ΔC_p also reduced by 0.46, 0.52, and 0.19 J g^{-1} °C^{-1} for the DEX+LD_5050, DEX+HD_5050, and DEX+LD_8515 samples, respectively. Unlike the LD_8515 sample, the cold crystallization peak was not present in the DEX+LD_8515 sample. The semi-crystalline LD_PLLA sample showed a T_g at 54.9 °C and T_m at 173 °C associated with a ΔH_m of 51.56 J g^{-1} (Figure 7d). Upon DEX addition, the T_g value decreased by 4.1 °C, while T_m reduced by 1.9 °C associated with a ΔH_m reduction of 3.72 J g^{-1}. Additionally, a cold crystallization peak at 82.9 °C and a melt-recrystallization peak at 149.5 °C were both observed for the LD_PLLA samples, which shifted by 1.3 °C (associated with a ΔH_{cc} change of 0.77 J g^{-1}) and 2.1 °C (associated with a ΔH_{mc} change of 1.28 J g^{-1}), respectively, in the DEX+LD_PLLA samples. Importantly, the DEX +LD_PLLA samples also exhibited a 1.83% reduction in crystallinity compared to LD_PLLA. In contrast, the LD_PCL samples showed no significant change in T_m, ΔH_m, and percent crystallinity with DEX addition (Figure 7e). A summary of key thermal properties obtained from DSC analysis is presented in Table 1.

2.6. Evaluation of In Vitro Release Kinetics of DEX from Electrospun Meshes. The calibration curve used for determining DEX release in this study (λ_{max} = 240 nm) is presented in Figure S5, Supporting Information. The optimized drug loading used in this study was chosen by conducting pilot release studies at different drug loadings. Some of these results are presented in Figure S6, Supporting Information. In these initial studies, the PCL meshes were found to exhibit burst release regardless of the loading, while the PLGA 85:15 and PLLA meshes exhibited negligible release when the drug concentration was 5.5 mg DEX/mL of polymer solution. Based on these results, a concentration of 8.5 mg DEX/mL of polymer solution was chosen to result in differential release kinetics across the groups while still remaining within the therapeutic window to potentially promote favorable biological responses.

Table 1. Summary of Important Thermal Properties Obtained from DSC

experimental group	T_g (°C)	ΔC_p (J g^{-1} °C^{-1})	T_m (°C)	ΔH_m (J g^{-1})	% crystallinity
LD_5050	39.5	1.13			
DEX+LD_5050	35.3	0.67			
HD_5050	36.7	0.92			
DEX+HD_5050	32.8	0.39			
LD_8515	40.3	0.80			
DEX+LD_8515	37.2	0.61			
LD_PLLA	54.9		173	51.56	30.20
DEX+LD_PLLA	50.8		171.1	47.84	28.37
LD_PCL			60.4	71.72	51.60
DEX+LD_PCL			60.5	71.70	51.58

In the final release experiments, encapsulation efficiency within the optimized DEX-loaded mesh samples was determined by using a solvent extraction/precipitation method to recover the total amount of DEX present within each sample. Thereafter, the actual amount of DEX incorporated into the samples post-electrospinning relative to the theoretical amount loaded was calculated and determined to be greater than 90% in all samples (Figure S7, Supporting Information). The in vitro cumulative release of DEX from the meshes—normalized by both the dry weight of the meshes and the encapsulation efficiency—was monitored for a period of 28 days (Figure 8). DEX+LD_PCL samples demonstrated a burst release of 65% within the first 6 h and a cumulative release of 98% within 24 h. The DEX+LD_5050 samples exhibited a sharp release of around 39% over 3 days followed by sustained release over the rest of the study. In contrast, the rate of DEX release from the DEX+HD_5050 samples was significantly slower ($p < 0.01$) than the DEX+LD_5050 samples over the first 7 days, following which the DEX release rate increased between days 7 and 14. Nevertheless, as with the DEX +LD_5050 samples, close to 100% of the drug was released from the DEX+HD_5050 samples by the end of the study. In contrast, a much more sustained and controlled release of DEX was observed from the DEX+LD_8515 samples, with only 26% of the total drug released by day 28. The cumulative

https://dx.doi.org/10.1021/acsomega.0c00954
ACS Omega 2020, 5, 15865−15876

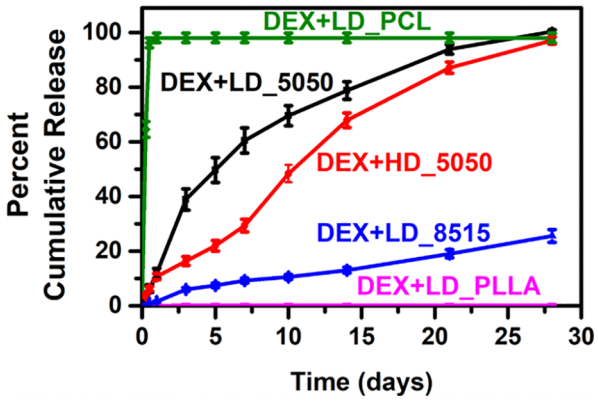

Figure 8. Percent cumulative release of DEX from electrospun meshes over 28 days.

release of drug from the DEX+LD_PLLA was negligible over the entire duration of the study.

In order to theoretically predict possible release mechanisms from the fibrous meshes, the release data were fitted to phenomenologically relevant Korsmeyer–Peppas (KP) and Higuchi models. Respective parameters corresponding to the best fit are presented in Table 2. The release data for the DEX +LD_5050, DEX+HD_5050, DEX+LD_8515, and DEX +LD_PCL fit best with the KP model. While an anomalous transport mechanism was predicted for release from DEX +LD_5050 and DEX+LD_8515 samples ($0.45 < n < 0.89$), drug release from DEX+HD_5050 samples was predicted to follow a super case II transport mechanism ($n > 0.89$). Drug release from the DEX+LD_PLLA fits better with the Higuchi model.

Table 2. Best-Fit Parameters Obtained for Drug Release from Electrospun Meshes

experimental group	model and parameters	R^2
DEX+LD_5050	k = 0.161, n = 0.661 (KP model)	0.991
DEX+HD_5050	k = 0.053, n = 0.97 (KP model)	0.992
DEX+LD_8515	k = 0.098, n = 0.634 (KP model)	0.992
DEX+LD_PLLA	k = 0.007 (Higuchi model)	0.938
DEX+LD_PCL	k = 0.899, n = 0.224 (KP model)	1

3. DISCUSSION

A deeper understanding of critical matrix-related and associated factors guiding drug release can aid the rational design of scaffolds for several biomedical applications requiring sustained release while concurrently avoiding significant burst release (e.g., implantable drug-eluting materials to combat chronic inflammation). Accordingly, four poly α-esters—commonly employed in several tissue engineering and drug delivery applications[24]—were examined for their ability to release dexamethasone (DEX) over a period of 28 days in vitro. The operating parameters such as flow rate and throw distance used for electrospinning the polymeric solutions were carefully optimized in pilot studies and are similar to previous reports.[25−27] DEX loading was kept constant at 8.5 mg drug/mL polymer solution across the groups so as to maintain similar differences in initial drug concentration between the matrix and the release medium.[28] This DEX concentration—chosen based on pilot release experiments (Figure S6, Supporting Information)—is within the therapeutic window to exert possible biological effects on macrophages.[8,22,29] While biological assessment of the released DEX was not part of the current study, based on previous in vitro and in vivo reports of biological assessment,[7,30] the drug released from our matrices would be active over the time period investigated in our study. In fact, a commercially available DEX-loaded PLGA implant, Ozurdex, is known to release biologically active DEX over the course of a few months.[31] To enable direct comparison of DEX release across all experimental groups in our study, we normalized the amount of drug released by both the sample weight and the actual amount of drug initially present in each sample as determined from an assessment of the encapsulation efficiency (Figure S7, Supporting Information). While the slowly degrading PCL samples exhibited a burst release of 98% DEX within 24 h, the cumulative release of drug from the semi-crystalline PLLA samples was insignificant throughout the duration of the study. DEX+LD_5050 displayed a sharp initial release of 39% drug over 3 days followed by sustained release, while the release rate of DEX from the higher-diameter DEX +HD_5050 sample varied as a function of time. However, both samples released almost 100% drug by day 28. In contrast, DEX+LD_8515 released the drug in a controlled manner over the entire duration of the study.

To decouple the effects of fiber architecture from chemistry, DEX-loaded electrospun meshes were fabricated to possess similar architectures, viz., diameters (Figure 1) and porosities (Figure 2). The effect of fiber size on DEX release was evaluated by electrospinning only the PLGA 50:50 samples at two different polymer concentrations so as to result in significantly different fiber diameters (Figure 1f). Between days 1 and 7, the higher-diameter DEX+HD_5050 sample demonstrated a smaller cumulative release compared to the lower-diameter DEX+LD_5050 sample (Figure 8), attributable to differences in diffusional length scales. These results are consistent with previously reported studies evaluating the effect of fiber diameter on drug release.[32,33] However, the DEX +HD_5050 (and DEX+LD_PCL) also exhibited a higher thickness compared to the rest of the samples (Figure S3, Supporting Information) although these differences were not statistically significant. Despite using the same flow rate and deposition times for all samples, a higher thickness resulted from a smaller deposition area on the collector as reported previously for specific electrospinning jets.[34] Nevertheless, statistically insignificant differences in sample thicknesses likely had negligible influence on the release kinetics given the high porosity of the meshes (Figure 2) and the relatively large fiber diameters (Figure 1) compared to the size of the drug (392.5 Da).

Drug release from polymeric matrices can be affected by matrix wettability and consequent solvent diffusion into the matrices.[35] Traditional water contact angle measurements provide information only about surface properties that are not suitable for correlation with bulk drug release from polymeric matrices.[36] Therefore, in this study, we evaluated bulk wettability by measuring the hydrophobicity of matrices using a technique that relies upon solvent-induced swelling. Our hydrophobicity results for the PLGA samples (Figure 3) are consistent with Vargha-Butler et al. who showed that PLGA hydrophobicity is independent of the lactide-to-glycolide ratio.[37] In our study, the HD_5050 meshes displayed a slightly higher H-index than the LD_5050 meshes with the same composition although these differences were not statistically significant. These results suggest that solvent

https://dx.doi.org/10.1021/acsomega.0c00954
ACS Omega 2020, 5, 15865−15876

penetration and consequent swelling may be sensitive to differences in fiber sizes, an effect that can be studied in more detail by investigating the interaction of matrices possessing different architectures with solvents possessing different polarities. Despite this minor caveat, the release kinetics of hydrophobic DEX from the PLGA 50:50, PLGA 85:15, and PLLA were significantly different (Figure 8) although these matrices possessed similar H-indices. The results strongly indicate the involvement of other dominating factors driving drug release from these polymers. Additionally, despite possessing the highest H-index, the PCL meshes exhibited burst release of hydrophobic DEX (Figure 8) regardless of the DEX loading (Figure S6, Supporting Information), suggesting the absence of possible hydrophobic interactions that could have retarded the release.[38] Burst release of DEX from PCL meshes has also been reported in studies using different electrospinning solvents such as dichloromethane/dimethyl formamide[6] and chloroform/dimethyl formamide,[39] indicating that the use of TFE for electrospinning PCL in the present study likely had no significant influence on release kinetics. In summary, bulk hydrophobicity of the PCL matrices was not a critical factor influencing drug release.

Gross/microstructural changes to the mesh network upon soaking in PBS, providing direct visual evidence for polymer degradability, was another major factor that influenced drug release from the amorphous polymeric groups tested in this study. Previously, Li et al. have reported qualitative assessment of degradation in electrospun matrices;[40] however, the polymers used in their study possessed different molecular weights, which could have also influenced polymer degradation.[41] In our study, the four poly α-esters were carefully chosen to possess comparable M_n. Upon incubation in PBS at 37 °C, the LD_5050 and HD_5050 samples disintegrated completely by day 28 (Figure 4), consistent with bulk matrix degradation,[42] while the LD_8515 samples exhibited complete pore closure with minimal fiber fusion (Figure 5). These results are in agreement with the differences in the degradation time frames for PLGA 50:50 and PLGA 85:15 reported in the literature.[40,43] Next, we examined correlations between temporal changes in matrix morphology/microstructure and corresponding release kinetics of DEX. As noted previously, the DEX+HD_5050 samples exhibited a smaller cumulative release until day 7 as compared to the DEX+LD_5050 samples, primarily due to differences in fiber diameter and consequent differences in drug diffusion barriers. However, toward the later time points, fiber swelling and significant gross/microstructural changes to the network due to PBS penetration became dominant in both the DEX+LD_5050 and DEX+HD_5050 samples, resulting in 100% drug release by the end of the study. Comparatively, the slower-degrading DEX +LD_8515 samples released DEX in a controlled and sustained manner over 28 days. Together, these results reveal the temporal dependence of dominant factors driving the release of DEX from the PLGA matrices tested in this study. In contrast, both the semi-crystalline LD_PLLA and LD_PCL samples displayed neither gross (Figure 4) nor microstructural changes (Figure 5) even after 28 days of incubation in PBS, consistent with long degradation periods.[24] Despite these observations, the sharp burst release of DEX from DEX +LD_PCL (Figure 8) indicates that another factor—not slow fiber degradation—was responsible for drug release from PCL.

Thermal properties for the DEX-loaded matrices as well as control samples were measured to correlate shifts in endothermic/exothermic peaks and changes in ΔH and ΔC_p values with changes in percent crystallinity/amorphous content[8,44,45] and drug-polymer interactions.[46] Following DEX incorporation into the PLGA meshes, a reduction in T_g and ΔC_p values indicated a reduction in the amorphous content of these samples (Table 1), suggesting possible interactions. Analysis of Hansen solubility parameters available in the literature predicted miscibility of the drug ($\Delta\delta_t$ < 7 MPa$^{1/2}$)[47,48] with the PLGA matrices, with $\Delta\delta_t$ values for DEX-PLGA 50:50 and DEX-PLGA 85:15 being 5.6 MPa$^{1/2}$ and 3.8 MPa$^{1/2}$, respectively (Table S2, Supporting Information). These results also complement the findings of a previous report by Panyam et al. who showed that the solid-state solubility of DEX increased with an increase in lactide content.[49] As with the amorphous polymers, DSC analysis of the semi-crystalline PLLA revealed a reduction in T_g and T_m (Figure 7d), as well as a simultaneous lowering of enthalpies for cold crystallization, melt-recrystallization, and melting upon the addition of DEX (Table 1). These results along with a 1.83% reduction in crystallinity for the DEX+LD_PLLA samples compared to LD_PLLA indicate interactions of DEX with PLLA. Moreover, the reduction in percent crystallinity is not insignificant,[8] given the low DEX loading used in the study. Unlike PLLA, PCL displayed no significant changes in T_m, ΔH_m, or percent crystallinity after DEX incorporation (Figure 7e), indicating negligible drug-polymer interactions. While ATR-FTIR spectra (Figure 6a−e) did not reveal significant peak shifts for any of the groups (likely due to the beam penetration depth relative to fiber size and the low DEX loading), the characteristic DEX peak at 1666.39 cm^{-1} was observed in all groups and is consistent with spectra for DEX powder previously reported.[50] Interestingly, other peaks for the C═C bonds in DEX were observed only in the DEX-loaded PCL meshes but not in the DEX-loaded PLGA and PLLA samples (Figure 6f). Indeed, high-magnification SEM micrographs revealed phase-separated DEX crystallites only on the surface of DEX+LD_PCL fibers (Figure S2, Supporting Information) and not in any of the other DEX-loaded polymers. Consistent with these observations, analysis of theoretical drug-polymer miscibility based on Hansen solubility values obtained from the literature (Table S2, Supporting Information) predicted partial drug miscibility in PCL ($\Delta\delta_t$ of DEX-PCL = 9.4 MPa$^{1/2}$) and full miscibility for the drug in PLLA ($\Delta\delta_t$ of DEX-PLLA < 7 MPa$^{1/2}$).[47,48] Taken together, our data for DEX+LD_PCL and DEX+LD_PLLA meshes along with the theoretical predictions of drug-polymer miscibility correlate well with the release profiles of DEX observed (Figure 8). While sustained release of DEX has been previously demonstrated from PCL scaffolds prepared using lyophilization and compression,[51] our results for burst release from PCL matrices prepared by electrospinning are consistent with previous reports.[6,22] We suggest that release kinetics from electrospun matrices can be better understood through an investigation of relevant matrix properties (e.g., hydrophobicity, mesh architecture, matrix degradability), along with the examination of drug-polymer miscibility and possible interactions.

To theoretically investigate differences in the release mechanisms across the five drug-polymer systems, the release profiles were fitted to the Korsmeyer−Peppas and Higuchi models (Table 2). Other models (e.g., Hixson−Crowell) were not used due to their assumptions that are not relevant for the matrices tested in this study.[52] The release profiles of DEX

https://dx.doi.org/10.1021/acsomega.0c00954
ACS Omega 2020, 5, 15865−15876

from PLGA 50:50, PLGA 85:15, and PCL fit best to the Korsmeyer–Peppas model. This model considers diffusion of release medium into the matrix, diffusion of drug out of the matrix, matrix swelling, and dissolution to explain mechanisms based on exponents obtained. As expected, the model predicted Fickian diffusion for release of drug from DEX +LD_PCL at a very high release rate, which agrees with our experimental findings. Non-Fickian mechanisms predicted for the PLGA matrices are in agreement with the ability of these matrices to swell and degrade in aqueous environments. However, the release of DEX from PLLA fitted better with the Higuchi model wherein drug diffusivity is assumed to be constant and polymer swelling and dissolution are considered negligible.

While our study enables developing meshes with various combinations of matrix properties that can promote DEX release over different timescales, specific choice of mesh properties depends upon intended applications. For example, induction of osteoblastic differentiation in vitro with DEX[30] may be achieved by using the DEX+LD_5050 meshes that release 80% of the drug within two weeks. However, for combating chronic inflammation in vivo,[7] DEX+LD_8515 or DEX+LD_PLLA that show potential for controlled release over several weeks to possibly a few months may be used. We suggest that the findings from the present study can also be used to design matrices for the release of drugs belonging to the same class as DEX, viz., glucocorticoids, as well as drugs possessing similar molecular weights (which would determine diffusion) and solid-state solubility/drug-polymer miscibility (which would be determined by drug-polymer interactions).

4. CONCLUSIONS

In this study, the slowest-degrading polymer PCL—with poor drug-polymer miscibility and exhibiting negligible interactions with DEX—released close to 98% DEX within 24 h. Stronger DEX-polymer interactions, full drug-polymer miscibility, and negligible matrix degradability led to no appreciable release of DEX from the PLLA samples over four weeks. The release from the PLGA samples was influenced by a combination of matrix architecture, fiber swelling, gross/microstructural changes to the mesh network (consistent with degradation), and solid-state drug solubility, wherein the dominant driving factor changed as time progressed. In summary, our study shows that a deeper understanding of the correlations between specific combinations of matrix properties and drug release kinetics along with associated mechanisms of release can help establish rational design criteria for matrices used in controlled release applications. We conclude that the PLGA 85:15 with a specific combination of matrix properties evaluated in this study—not the slowest-degrading PCL as would be expected—may be suitable to achieve localized, controlled, and sustained release of DEX to potentially combat chronic inflammation.

5. METHODS

5.1. Materials. All plasticware and laboratory supplies were purchased from Tarsons Products, India unless otherwise specified. Ester-terminated poly(D,L-lactide-*co*-glycolide) 50:50 (PLGA 50:50, M_n = 65.5 kDa), ester-terminated poly(D,L-lactide-*co*-glycolide) 85:15 (PLGA 85:15, M_n = 75.8 kDa), and ester-terminated poly(L-lactide) (PLLA, M_n = 77.5 kDa) were purchased from LACTEL Absorbable Polymers, USA. Polycaprolactone (PCL, M_n = 80 kDa), 2,2,2-trifluoroethanol (TFE, ≥99% (GC)), 1,1,1,3,3,3-hexafluoro-2-propanol (HFIP, ≥99% (GC)), and hydrophobic dexamethasone (DEX, ≥98% (HPLC), powder) were purchased from Sigma-Aldrich, USA. Methanol (≥99.7% (GC)) and phosphate-buffered saline (PBS) were obtained from HiMedia Laboratories, India, while 2-propanol (≥99.5%) was obtained from Sisco Research Laboratories, India.

5.2. Fabrication of DEX-Loaded Fibrous Meshes via Electrospinning. To fabricate DEX-loaded fibrous meshes, polymer solutions were first prepared by dissolving PCL in TFE at 12.5% (w/v), PLLA in HFIP at 21.5% (w/v), PLGA 85:15 in HFIP at 21.5% (w/v), and PLGA 50:50 in HFIP at 20.5% (w/v). Polymer concentrations were chosen judiciously in order to obtain similar fiber diameters across the experimental groups and thus avoid significant differences in matrix architecture from influencing drug release. To specifically evaluate the effect of mesh architecture on drug release, PLGA 50:50 was separately dissolved in HFIP at 25.5% (w/v) to obtain a significantly larger fiber diameter compared to the other samples. All polymer solutions were allowed to stir for 48 h followed by the addition of methanol-reconstituted DEX at an optimized concentration of 8.5 mg drug/mL of polymer solution. DEX was soluble in methanol, TFE, and HFIP at 25 mg/mL (25 °C), which ensured that the drug loading used was within the solubility limits. After stirring overnight, the DEX-incorporated solutions were sonicated with a probe tip sonicator (Qsonica, USA) for 30 s and immediately loaded into 5 mL syringes capped with 21-gauge blunt tip needles (VWR International, USA). DEX-incorporated solutions were electrospun under ambient conditions using a custom-designed electrospinning unit (E-Spin Nanotech, India), and samples were collected for a total of 60 min on a grounded metal collector wrapped in aluminum foil. All meshes were allowed to dry in a fume hood and further degassed in a desiccator overnight to remove residual solvent. Control polymer meshes without DEX were separately prepared in a similar manner. The electrospinning parameters for the various experimental groups prepared in this study are presented in Table S1, Supporting Information.

For characterization and drug release studies, circular samples of 1.5 cm diameter were punched from all fibrous meshes using a chrome-plated steel cork borer (Cole-Parmer, USA). DEX-incorporated samples were designated DEX +LD_5050, DEX+LD_8515, DEX+LD_PLLA, and DEX +LD_PCL and corresponded to DEX-loaded PLGA 50:50, PLGA 85:15, PLLA, and PCL, respectively, all possessing similar average fiber diameters. DEX-loaded PLGA 50:50 meshes, prepared using a significantly higher concentration of 25.5% (w/v) and consequently possessing a significantly higher diameter than the rest of the samples, were designated DEX +HD_5050.

5.3. Scanning Electron Microscopy (SEM). Fiber morphology and diameter distribution of DEX-loaded electrospun meshes were determined using SEM. Briefly, samples were mounted on a metal substrate with carbon tape (Ted Pella, USA) and sputter-coated (Quorum Technologies, UK) with Au/Pd for 120 s using a 15 mA process current. Sputter-coated samples were imaged at an accelerating voltage of 10 kV using a tabletop SEM (Phenom World, Netherlands) fitted with a backscatter electron detector. ImageJ software (National Institutes of Health, USA) was used to measure the diameters of at least 100 fibers per sample collected across several SEM

https://dx.doi.org/10.1021/acsomega.0c00954
ACS Omega 2020, 5, 15865−15876

micrographs, and histograms were generated using OriginPro9 software (OriginLab Corporation, USA).

5.4. Evaluation of Mesh Porosity. The porosity of DEX-loaded electrospun meshes was determined using a gravimetric method as reported previously.[53] Briefly, the thickness of 1.5 cm circular samples was measured using an inverted microscope (Nikon Instruments, Japan), and the apparent density of the scaffold ($\rho_{apparent}$) was calculated from the measured weight of the samples. Using a known density of the polymer ($\rho_{polymer}$), the porosity of the meshes was determined by eq 1

$$\text{Porosity} = 1 - \frac{\rho_{apparent}}{\rho_{polymer}} \quad (1)$$

5.5. Measurement of Bulk Hydrophobicity. Relative hydrophobicity of electrospun meshes was measured using an adaptation of a technique reported previously.[36] This approach relies upon differential swelling of polymeric samples in solvents possessing distinct polarities. Briefly, dry weights (W_D) of 1.5 cm circular samples were measured, following which they were immersed separately in excess of either ultrapure water or 2-propanol and allowed to equilibrate at room temperature. Following solvent-induced swelling to equilibrium, swollen weights (W_S) were measured and used to calculate a hydrophobicity index (H-index)—an indicator of relative bulk hydrophobicity—using eq 2

$$\text{H} - \text{index} = \frac{(W_S/W_D)_{2-\text{propanol}}}{(W_S/W_D)_{\text{water}}} \quad (2)$$

5.6. Evaluation of Gross and Microstructural Changes to Meshes upon PBS Incubation: Qualitative Assessment of Mesh Degradation. Degradation of the electrospun meshes was qualitatively assessed by tracking gross changes in sample size/shape as well as microscopic changes in fiber morphology following incubation in an aqueous buffer. Briefly, electrospun samples were placed in microcentrifuge tubes containing 2 mL of PBS and secured on an orbital shaker inside an incubator (Symbiogen Biotechnologies Pvt. Ltd., India) at 37 °C. At specific predetermined time points, samples were retrieved from the buffer and images were captured using a color camera, following which fresh PBS was added to the samples, and the study continued for a total of 28 days. Concurrently, samples were also collected at days 1, 3, 7, and 28 and imaged under SEM in order to microscopically assess the extent of pore closure and fiber degradation.

5.7. Attenuated Total Reflectance-Fourier Transform Infrared Spectroscopy (ATR-FTIR). Electrospun meshes, with and without DEX, were analyzed using ATR-FTIR (Bruker Corporation, USA) to confirm drug presence. Briefly, samples were mounted on the crystal plate assembly, and all spectra were collected in the 600−3200 cm^{-1} range using a resolution of 4 cm^{-1} for a total of 256 scans.

5.8. Thermogravimetric Analysis (TGA). TGA was performed on the control electrospun meshes using a thermogravimetric analyzer (PerkinElmer, USA) to determine moisture content and the temperature of the onset of decomposition. Briefly, 10 mg electrospun samples were heated from ambient temperature to 550 °C at a ramp rate of 10 °C min^{-1} under a continuous nitrogen flow of 20 mL min^{-1}, and weight percentage was plotted as a function of temperature.

5.9. Differential Scanning Calorimetry (DSC). Electrospun meshes, with and without DEX, were analyzed using DSC (TA instruments, USA) to evaluate the glass transition temperature (T_g), melting temperature (T_m), and changes in enthalpy or specific heat capacity (ΔC_p) as applicable. Briefly, 10 mg electrospun samples were heated from 25 to 200 °C at a rate of 10 °C min^{-1} under a continuous nitrogen flow of 50 mL min^{-1}, and percent crystallinity of the LD_PLLA and LD_PCL samples was determined using eq 3

$$\%\ \text{Crystallinity} = \frac{\Delta H_m - \Delta H_{cc,mc}}{\Delta H_m{}^\circ} \quad (3)$$

where ΔH_m is the enthalpy of melting, $\Delta H_{cc,mc}$ is the enthalpy of cold crystallization and/or melt-recrystallization, and $\Delta H_m{}^\circ$ is the melting enthalpy for a 100% crystalline sample, viz., 139 J g^{-1} for PCL[54] and 91 J g^{-1} for PLLA.[55]

5.10. Theoretical Prediction of Drug-Polymer Miscibility. To support the experimental data, Hansen solubility parameters were obtained from the literature for the drug and polymers tested in this study,[56−58] and theoretical prediction of drug-polymer miscibility was calculated. These details are presented in the Supporting Information under "Analysis of Hansen solubility parameters" and Table S2.

5.11. Encapsulation Efficiency of DEX within Electrospun Meshes. Encapsulation efficiency, i.e., the actual amount of DEX incorporated within the different samples post-electrospinning, was determined using a solvent precipitation method adapted from a previously reported technique.[59] Briefly, DEX-loaded circular samples of 1.5 cm diameter were dissolved in TFE, and following the addition of excess methanol, the solution was vortexed to fully precipitate the polymer and extract the DEX into solution. Thereafter, the suspensions were centrifuged at 13000 rpm (Thermo Scientific, USA) for 15 min, and the supernatant containing the DEX was evaporated. Subsequently, the DEX was reconstituted, and the absorbance of the solutions was measured within ultraviolet-light-compatible 96 well microplates (Corning Inc., USA) using a microplate reader (BioTek Instruments Inc., USA) operating at a wavelength of 240 nm. The percent encapsulation efficiency (%EE) was calculated using eq 4

$$\%\text{EE} = \frac{\text{Actual amount of DEX present in each mesh}}{\text{Theoretical amount of DEX in each mesh}} \times 100 \quad (4)$$

5.12. In Vitro Release of DEX from Electrospun Meshes. To determine the release of DEX from the various electrospun meshes, 1.5 cm diameter circular samples were immersed in 2 mL of PBS and secured on an orbital shaker inside an incubator at 37 °C. At specific time points over the course of 4 weeks, the entire PBS was collected and equal volume of fresh PBS was added in order to maintain infinite sink conditions. At each time point, the recovered releasate was stored at 4 °C, while the release study was continued for 28 days. Control samples were also treated in a similar manner to determine background from the polymeric meshes without DEX. At the end of the study, the amount of DEX in the releasates collected at each time point was measured using a microplate reader operating at a wavelength of 240 nm. Absorbance was correlated with concentration of DEX using the linear portion of a calibration curve. DEX concentrations thus obtained were normalized by both the dry weights of the meshes and the actual initial amount of DEX present in each sample. To assess possible differences in release mechanisms,

https://dx.doi.org/10.1021/acsomega.0c00954
ACS Omega 2020, 5, 15865−15876

the experimental data were fitted to phenomenologically relevant models, namely, the Korsmeyer–Peppas and Higuchi[52] given by eqs 5 and 6, respectively

$$\frac{M_t}{M_\infty} = kt^n \tag{5}$$

where M_t/M_∞ is the fraction of drug released at time t, k is the release rate constant, and n is the release exponent.

$$Q_t = kt^{0.5} \tag{6}$$

where Q_t is the amount of drug released in time t, and k is the Higuchi dissolution constant. Results are presented for the best fit for each experimental group.

5.13. Statistical Analysis. Results are reported as mean ± standard deviation and correspond to $n > 100$ samples for fiber diameter analysis collected across several SEM micrographs per sample, $n = 3$ samples for thickness/porosity measurements, relative bulk hydrophobicity, and encapsulation efficiency, and $n = 5$ for DEX release from fibrous meshes. For ATR-FTIR and DSC, measurements were obtained over at least two independent runs and representative spectra and thermal data are presented. Statistical analysis was performed using a one-way ANOVA and Tukey post hoc test on OriginPro9 software (OriginLab Corporation, USA) with $p \leq 0.01$ considered statistically significant.

■ ASSOCIATED CONTENT

Supporting Information

The Supporting Information is available free of charge at https://pubs.acs.org/doi/10.1021/acsomega.0c00954.

Electrospinning parameters, Hansen solubility parameter analysis, fiber diameter distribution of DEX-loaded electrospun meshes, high-magnification SEM micrographs of (a) LD_PCL and (b) DEX+LD_PCL meshes, mesh thicknesses of DEX-incorporated electrospun meshes, TGA curves, DEX calibration curve, DEX release from meshes at different DEX loadings, and encapsulation efficiency of DEX in the electrospun meshes (PDF)

■ AUTHOR INFORMATION

Corresponding Author

Satyavrata Samavedi – *Department of Chemical Engineering, Indian Institute of Technology Hyderabad, Hyderabad 502285, India;* orcid.org/0000-0003-1196-1598; Phone: +91-40-23016216; Email: samavedi@che.iith.ac.in; Fax: +91-40-23016032

Author

Nikhita Joy – *Department of Chemical Engineering, Indian Institute of Technology Hyderabad, Hyderabad 502285, India;* orcid.org/0000-0001-8166-6151

Complete contact information is available at: https://pubs.acs.org/10.1021/acsomega.0c00954

Notes

The authors declare no competing financial interest.

■ ACKNOWLEDGMENTS

This work was supported by the Science and Engineering Research Board, Department of Science and Technology, India (grant number ECR/2016/000132). The authors gratefully acknowledge the research facilities provided by the Indian Institute of Technology Hyderabad, India. Some micrographs in this manuscript were obtained with the help of a SEM procured through a grant (grant number SR/FST/ETI-421/2016) to the Materials Science and Engineering Department, Indian Institute of Technology Hyderabad.

■ REFERENCES

(1) Pahwa, R.; Jialal, I. *Chronic Inflammation*; StatPearls: Treasure Island (FL), 2019.

(2) Nathan, C.; Ding, A. Nonresolving inflammation. *Cell* **2010**, *140*, 871–882.

(3) Oray, M.; Abu Samra, K.; Ebrahimiadib, N.; Meese, H.; Foster, C. S. Long-term side effects of glucocorticoids. *Expert Opin Drug Saf* **2016**, *15*, 457–465.

(4) Twaites, B.; de las Heras Alarcón, C.; Alexander, C. Synthetic polymers as drugs and therapeutics. *J. Mater. Chem.* **2005**, *15*, 441–455.

(5) Catalin Balaure, P.; Mihai Grumezescu, A. Smart synthetic polymer nanocarriers for controlled and site-specific drug delivery. *Curr. Top. Med. Chem.* **2015**, *15*, 1424–1490.

(6) Rubert, M.; Li, Y.-F.; Dehli, J.; Taskin, M. B.; Besenbacher, F.; Chen, M. Dexamethasone encapsulated coaxial electrospun PCL/PEO hollow microfibers for inflammation regulation. *RSC Adv.* **2014**, *4*, 51537–51543.

(7) Gu, B.; Wang, Y.; Burgess, D. J. In vitro and in vivo performance of dexamethasone loaded PLGA microspheres prepared using polymer blends. *Int. J. Pharm.* **2015**, *496*, 534–540.

(8) Vacanti, N. M.; Cheng, H.; Hill, P. S.; Guerreiro, J. D. T.; Dang, T. T.; Ma, M.; Watson, S.; Hwang, N. S.; Langer, R.; Anderson, D. G. Localized delivery of dexamethasone from electrospun fibers reduces the foreign body response. *Biomacromolecules* **2012**, *13*, 3031–3038.

(9) Chou, S. F.; Carson, D.; Woodrow, K. A. Current strategies for sustaining drug release from electrospun nanofibers. *J. Controlled Release* **2015**, *220*, 584.

(10) Li, S.; Vert, M. Biodegradation of aliphatic polyesters. In *Degradable polymers*; Springer: 2002; pp 71–131.

(11) Gavasane, A. J.; Pawar, H. A. Synthetic biodegradable polymers used in controlled drug delivery system: an overview. *Clin. Pharmacol. Biopharm.* **2014**, *3*, 1–7.

(12) Meinel, A. J.; Germershaus, O.; Luhmann, T.; Merkle, H. P.; Meinel, L. Electrospun matrices for localized drug delivery: current technologies and selected biomedical applications. *Eur. J. Pharm. Biopharm.* **2012**, *81*, 1–13.

(13) Ji, W.; Sun, Y.; Yang, F.; van den Beucken, J. J. J. P.; Fan, M.; Chen, Z.; Jansen, J. A. Bioactive electrospun scaffolds delivering growth factors and genes for tissue engineering applications. *Pharm. Res.* **2011**, *28*, 1259–1272.

(14) Moydeen, A. M.; Ali Padusha, M. S.; Aboelfetoh, E. F.; Al-Deyab, S. S.; El-Newehy, M. H. Fabrication of electrospun poly(vinyl alcohol)/dextran nanofibers via emulsion process as drug delivery system: Kinetics and in vitro release study. *Int. J. Biol. Macromol.* **2018**, *116*, 1250–1259.

(15) Carson, D.; Jiang, Y.; Woodrow, K. A. Tunable Release of Multiclass Anti-HIV Drugs that are Water-Soluble and Loaded at High Drug Content in Polyester Blended Electrospun Fibers. *Pharm. Res.* **2016**, *33*, 125–136.

(16) Gasmi, H.; Siepmann, F.; Hamoudi, M. C.; Danede, F.; Verin, J.; Willart, J.-F.; Siepmann, J. Towards a better understanding of the different release phases from PLGA microparticles: Dexamethasone-loaded systems. *Int. J. Pharm.* **2016**, *514*, 189–199.

(17) Lee, J. W.; Lee, H. Y.; Park, S. H.; Park, J. H.; Kim, J. H.; Min, B. H.; Kim, M. S. Preparation and Evaluation of Dexamethasone-Loaded Electrospun Nanofiber Sheets as a Sustained Drug Delivery System. *Materials* **2016**, *9*, 175.

(18) Mishra, D.; Kang, H. C.; Cho, H.; Bae, Y. H. Dexamethasone-Loaded Reconstitutable Charged Polymeric (PLGA) n-b-bPEI

Micelles for Enhanced Nuclear Delivery of Gene Therapeutics. *Macromol. Biosci.* **2014**, *14*, 831−841.
(19) Bode, C.; Kranz, H.; Siepmann, F.; Siepmann, J. In-situ forming PLGA implants for intraocular dexamethasone delivery. *Int. J. Pharm.* **2018**, *548*, 337−348.
(20) Wang, Q.; Wang, J.; Lu, Q.; Detamore, M. S.; Berkland, C. Injectable PLGA based colloidal gels for zero-order dexamethasone release in cranial defects. *Biomaterials* **2010**, *31*, 4980−4986.
(21) Kharaziha, M.; Fathi, M. H.; Edris, H.; Nourbakhsh, N.; Talebi, A.; Salmanizadeh, S. PCL-forsterite nanocomposite fibrous membranes for controlled release of dexamethasone. *J. Mater. Sci. Mater. Med.* **2015**, *26*, 5364.
(22) Li, Y.-F.; Rubert, M.; Yu, Y.; Besenbacher, F.; Chen, M. Delivery of dexamethasone from electrospun PCL−PEO binary fibers and their effects on inflammation regulation. *RSC Adv.* **2015**, *5*, 34166−34172.
(23) Kumar, A.; Pillai, J. Implantable drug delivery systems: An overview. In *Nanostructures for the Engineering of Cells, Tissues and Organs*; Elsevier: 2018; pp 473−511.
(24) Washington, K. E.; Kularatne, R. N.; Karmegam, V.; Biewer, M. C.; Stefan, M. C. Recent advances in aliphatic polyesters for drug delivery applications. *Wiley Interdiscip. Rev. Nanomed. Nanobiotechnol.* **2017**, *9*, No. e1446.
(25) Valizadeh, A.; Bakhtiary, M.; Akbarzadeh, A.; Salehi, R.; Frakhani, S. M.; Ebrahimi, O.; Rahmati-yamchi, M.; Davaran, S. Preparation and characterization of novel electrospun poly (ε-caprolactone)-based nanofibrous scaffolds. *Artif. Cells, Nanomed., Biotechnol.* **2016**, *44*, 504−509.
(26) You, Y.; Min, B. M.; Lee, S. J.; Lee, T. S.; Park, W. H. In vitro degradation behavior of electrospun polyglycolide, polylactide, and poly (lactide-co-glycolide). *J. Appl. Polym. Sci.* **2005**, *95*, 193−200.
(27) Ma, Y.; Song, J.; Almassri, H. N. S.; Zhang, D.; Zhang, T.; Cheng, Y.; Wu, X. Minocycline-loaded PLGA electrospun membrane prevents alveolar bone loss in experimental peridontitis. *Drug Delivery* **2020**, *27*, 151−160.
(28) Bonferoni, M. C.; Rossi, S.; Ferrari, F.; Bettinetti, G. P.; Caramella, C. Characterization of a diltiazem-lambda carrageenan complex. *Int. J. Pharm.* **2000**, *200*, 207−216.
(29) Bartneck, M.; Peters, F. M.; Warzecha, K. T.; Bienert, M.; van Bloois, L.; Trautwein, C.; Lammers, T.; Tacke, F. Liposomal encapsulation of dexamethasone modulates cytotoxicity, inflammatory cytokine response, and migratory properties of primary human macrophages. *Nanomedicine* **2014**, *10*, 1209−1220.
(30) Martins, A.; Duarte, A. R. C.; Faria, S.; Marques, A. P.; Reis, R. L.; Neves, N. M. Osteogenic induction of hBMSCs by electrospun scaffolds with dexamethasone release functionality. *Biomaterials* **2010**, *31*, 5875−5885.
(31) Whitcup, S. M.; Robinson, M. R. Development of a dexamethasone intravitreal implant for the treatment of noninfectious posterior segment uveitis. *Ann. N. Y. Acad. Sci.* **2015**, *1358*, 1−12.
(32) Xie, J.; Wang, C. H. Electrospun micro- and nanofibers for sustained delivery of paclitaxel to treat C6 glioma in vitro. *Pharm. Res.* **2006**, *23*, 1817−1826.
(33) Chen, S. C.; Huang, X. B.; Cai, X. M.; Lu, J.; Yuan, J.; Shen, J. The influence of fiber diameter of electrospun poly (lactic acid) on drug delivery. *Fibers Polym.* **2012**, *13*, 1120−1125.
(34) Li, N.; Qin, X. H.; Lin, L.; Wang, S. Y. The effects of spinning conditions on the morphology of electrospun jet and nonwoven membrane. *Polym. Eng. Sci.* **2008**, *48*, 2362−2366.
(35) Li, Y. F.; Rubert, M.; Aslan, H.; Yu, Y.; Howard, K. A.; Dong, M.; Besenbacher, F.; Chen, M. Ultraporous interweaving electrospun microfibers from PCL-PEO binary blends and their inflammatory responses. *Nanoscale* **2014**, *6*, 3392−3402.
(36) Munoz-Pinto, D. J.; Grigoryan, B.; Long, J.; Grunlan, M.; Hahn, M. S. An approach for assessing hydrogel hydrophobicity. *J. Biomed. Mater. Res. A* **2012**, *100*, 2855−2860.
(37) Vargha-Butler, E.; Kiss, E.; Lam, C.; Keresztes, Z.; Kalman, E.; Zhang, L.; Neumann, A. Wettability of biodegradable surfaces. *Colloid Polym. Sci.* **2001**, *279*, 1160−1168.
(38) Dai, L.; Yang, T.; He, J.; Deng, L.; Liu, J.; Wang, L.; Lei, J.; Wang, L. Cellulose-graft-poly (l-lactic acid) nanoparticles for efficient delivery of anti-cancer drugs. *J. Mater. Chem. B* **2014**, *2*, 6749−6757.
(39) Boroojen, F. R.; Mashayekhan, S.; Abbaszadeh, H.-A. The controlled release of dexamethasone sodium phosphate from bioactive electrospun PCL/gelatin nanofiber scaffold. *Iran. J. Pharm. Res.* **2019**, *18*, 111.
(40) Li, W. J.; Cooper, J. A., Jr.; Mauck, R. L.; Tuan, R. S. Fabrication and characterization of six electrospun poly(alpha-hydroxy ester)-based fibrous scaffolds for tissue engineering applications. *Acta Biomater.* **2006**, *2*, 377−385.
(41) Mittal, G.; Sahana, D. K.; Bhardwaj, V.; Ravi Kumar, M. N. V. Estradiol loaded PLGA nanoparticles for oral administration: effect of polymer molecular weight and copolymer composition on release behavior in vitro and in vivo. *J. Controlled Release* **2007**, *119*, 77−85.
(42) Gil-Castell, O.; Badia, J. D.; Ontoria-Oviedo, I.; Castellano, D.; Marco, B.; Rabal, A.; Bou, J. J.; Serra, A.; Monreal, L.; Blanes, M.; Sepúlveda, P.; Ribes-Greus, A. In vitro validation of biomedical polyester-based scaffolds: Poly (lactide- co- glycolide) as model-case. *Polym. Test.* **2018**, *66*, 256−267.
(43) Ramchandani, M.; Pankaskie, M.; Robinson, D. The influence of manufacturing procedure on the degradation of poly (lactide-co-glycolide) 85: 15 and 50: 50 implants. *J. Controlled Release* **1997**, *43*, 161−173.
(44) Lappalainen, M.; Pitkänen, I.; Harjunen, P. Quantification of low levels of amorphous content in sucrose by hyperDSC. *Int. J. Pharm.* **2006**, *307*, 150−155.
(45) Einfalt, T.; Planinšek, O.; Hrovat, K. Methods of amorphization and investigation of the amorphous state. *Acta Pharm.* **2013**, *63*, 305−334.
(46) Taepaiboon, P.; Rungsardthong, U.; Supaphol, P. Drug-loaded electrospun mats of poly (vinyl alcohol) fibres and their release characteristics of four model drugs. *Nanotechnology* **2006**, *17*, 2317.
(47) Greenhalgh, D. J.; Williams, A. C.; Timmins, P.; York, P. Solubility parameters as predictors of miscibility in solid dispersions. *J. Pharm. Sci.* **1999**, *88*, 1182−1190.
(48) Mohammad, M. A.; Alhalaweh, A.; Velaga, S. P. Hansen solubility parameter as a tool to predict cocrystal formation. *Int. J. Pharm.* **2011**, *407*, 63−71.
(49) Panyam, J.; Williams, D.; Dash, A.; Leslie-Pelecky, D.; Labhasetwar, V. Solid-state solubility influences encapsulation and release of hydrophobic drugs from PLGA/PLA nanoparticles. *J. Pharm. Sci.* **2004**, *93*, 1804−1814.
(50) Fraile, J. M.; Garcia-Martin, E.; Gil, C.; Mayoral, J. A.; Pablo, L. E.; Polo, V.; Prieto, E.; Vispe, E. Laponite as carrier for controlled in vitro delivery of dexamethasone in vitreous humor models. *Eur. J. Pharm. Biopharm.* **2016**, *108*, 83−90.
(51) Fialho, S. L.; Behar-Cohen, F.; Silva-Cunha, A. Dexamethasone-loaded poly (ε-caprolactone) intravitreal implants: A pilot study. *Eur. J. Pharm. Biopharm.* **2008**, *68*, 637−646.
(52) Dash, S.; Murthy, P. N.; Nath, L.; Chowdhury, P. Kinetic modeling on drug release from controlled drug delivery systems. *Acta Pol Pharm* **2010**, *67*, 217−223.
(53) Pham, Q. P.; Sharma, U.; Mikos, A. G. Electrospun poly(epsilon-caprolactone) microfiber and multilayer nanofiber/microfiber scaffolds: characterization of scaffolds and measurement of cellular infiltration. *Biomacromolecules* **2006**, *7*, 2796−2805.
(54) Chasin, M. *Biodegradable polymers as drug delivery systems*; Informa Health Care: 1990; Vol. *45*.
(55) Pyda, M.; Bopp, R.; Wunderlich, B. Heat capacity of poly (lactic acid). *J. Chem. Thermodyn.* **2004**, *36*, 731−742.
(56) Lübtow, M. M.; Haider, M. S.; Kirsch, M.; Klisch, S.; Luxenhofer, R. Like Dissolves Like? A Comprehensive Evaluation of Partial Solubility Parameters to Predict Polymer−Drug Compatibility in Ultrahigh Drug-Loaded Polymer Micelles. *Biomacromolecules* **2019**, *20*, 3041−3056.
(57) Schenderlein, S.; Lück, M.; Müller, B. W. Partial solubility parameters of poly (D, L-lactide-co-glycolide). *Int. J. Pharm.* **2004**, *286*, 19−26.

(58) Adamska, K.; Voelkel, A.; Berlińska, A. The solubility parameter for biomedical polymers—Application of inverse gas chromatography. *J. Pharm. Biomed. Anal.* **2016**, *127*, 202−206.
(59) Xue, J.; He, M.; Liu, H.; Niu, Y.; Crawford, A.; Coates, P. D.; Chen, D.; Shi, R.; Zhang, L. Drug loaded homogeneous electrospun PCL/gelatin hybrid nanofiber structures for anti-infective tissue regeneration membranes. *Biomaterials* **2014**, *35*, 9395−9405.

https://dx.doi.org/10.1021/acsomega.0c00954
ACS Omega 2020, 5, 15865−15876